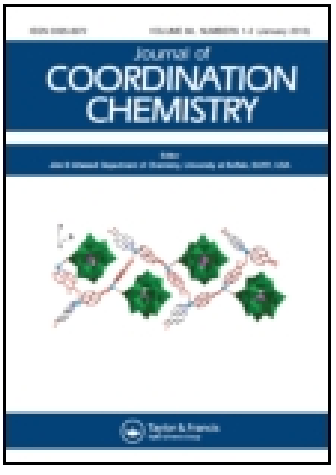

Journal of Coordination Chemistry
Publication details, including instructions for authors and subscription information:
http://www.tandfonline.com/loi/gcoo20

Three 2-(4-thiazolyl)benzimidazole-based supramolecular assemblies oriented by Keggin and Wells-Dawson anions

Ai-Xiang Tian[a], Yang Yang[a], Na Sun[b], Jia-Chen Li[a], Jun Ying[a], Ju-Wen Zhang[a] & Xiu-Li Wang[a]

[a] Department of Chemistry, Bohai University, Jinzhou, PR China

[b] Department of Chemical and Environmental Engineering, Hebei Chemical & Pharmaceutical Vocational Technology College, Shijiazhuang, PR China

Accepted author version posted online: 13 May 2014.Published online: 09 Jun 2014.

To cite this article: Ai-Xiang Tian, Yang Yang, Na Sun, Jia-Chen Li, Jun Ying, Ju-Wen Zhang & Xiu-Li Wang (2014) Three 2-(4-thiazolyl)benzimidazole-based supramolecular assemblies oriented by Keggin and Wells-Dawson anions, Journal of Coordination Chemistry, 67:9, 1550-1561, DOI: 10.1080/00958972.2014.923847

To link to this article: http://dx.doi.org/10.1080/00958972.2014.923847

Journal of Coordination Chemistry, 2014
Vol. 67, No. 9, 1550–1561, http://dx.doi.org/10.1080/00958972.2014.923847

Three 2-(4-thiazolyl)benzimidazole-based supramolecular assemblies oriented by Keggin and Wells–Dawson anions

AI-XIANG TIAN†*, YANG YANG†, NA SUN‡, JIA-CHEN LI†, JUN YING†, JU-WEN ZHANG† and XIU-LI WANG†*

†Department of Chemistry, Bohai University, Jinzhou, PR China
‡Department of Chemical and Environmental Engineering, Hebei Chemical & Pharmaceutical Vocational Technology College, Shijiazhuang, PR China

(*Received 24 February 2014; accepted 11 April 2014*)

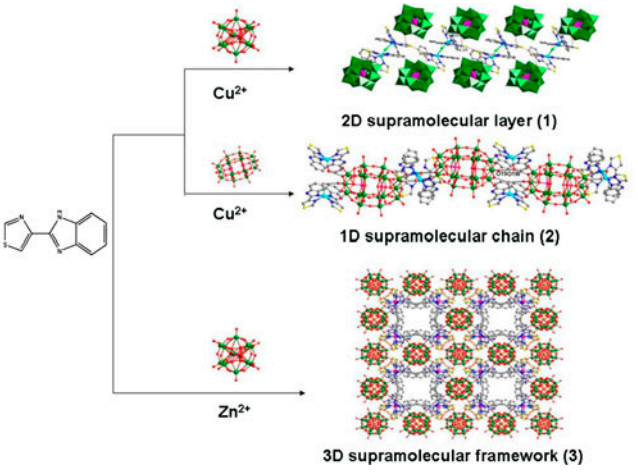

Three POM-based supramolecular compounds have been obtained under hydrothermal conditions. Compound **1** is a 2-D supramolecular layer, which is constructed from the binuclear copper clusters $\{Cu_2L_4Cl\}^{3+}$ and Keggin anions. Compound **2** exhibits a 1-D supramolecular chain built by Wells–Dawson anions and $[CuL_2(H_2O)]^{2+}$ subunits. In **3**, there exists an inorganic Keggin anion chain linked by K^+ ions and discrete $[Zn^{II}(L)_3]^{2+}$ subunits, which are connected by hydrogen bonding interactions to construct a 3-D supramolecular structure.

Three polyoxometalate supramolecular assemblies based on rigid 2-(4-thiazolyl)benzimidazole (**L**) and two types of polytungstate anions, $[Cu^{II}_2Cl(\mathbf{L})_4(PW_{12}O_{40})]\cdot 3H_2O$ (**1**), $[Cu^{II}(\mathbf{L})_2(H_2O)]_2[P_2W_{18}O_{62}]\cdot(H\mathbf{L})_2\cdot 6H_2O$ (**2**), and $[Zn^{II}(\mathbf{L})_3]_4[H(KPW_{12}O_{40})_3]$ (**3**), have been synthesized and characterized by single-crystal X-ray diffraction, elemental analyses, and IR spectra. Compound **1** contains binuclear copper clusters $\{Cu_2\mathbf{L}_4Cl\}^{3+}$ with Cl^- as bridges. These binuclear clusters and $[PW_{12}O_{40}]^{3-}$ anions construct a supramolecular 2-D layer through hydrogen-bonding interactions. In **2**, the $[Cu\mathbf{L}_2(H_2O)]^{2+}$ subunits and Wells–Dawson anions build a 1-D supramolecular chain. In **3**,

*Corresponding authors. Email: tian@bhu.edu.cn (A.-X. Tian); wangxiuli@bhu.edu.cn (X.-L. Wang)

the $[PW_{12}O_{40}]^{3-}$ anions are covalently linked by K^+ to form an inorganic chain. These chains and discrete $[Zn^{II}(\mathbf{L})_3]^{2+}$ subunits construct a 3-D supramolecular structure. The electrochemical and photocatalytic properties of **1**–**3** have been studied.

Keywords: Keggin polyoxometalate; Wells–Dawson polyoxometalate; Supramolecular assembly; 2-(4-Thiazolyl)benzimidazole; Electrochemical property

1. Introduction

Polyoxometalates (POMs) have been investigated owing to their large sizes [1], various shapes [2], and fascinating catalytic [3], electronic [4], and optical properties [5]. POMs have been extensively employed as important inorganic building blocks to construct novel hybrid materials combined with transition metal complexes (TMCs) [6, 7]. Many such compounds have been obtained, especially Keggin and Wells–Dawson-based structures [8–11]. In this series, POMs can play roles as inorganic linkages and supramolecular synthons [12]. The POM-based supramolecular compounds have attracted attention for properties, such as non-linear optics, catalysis, and medicine [13–15]. The high number of oxygens located on the spherical surface of POMs can supply hydrogen-bonding interactions with TMCs. Therefore, these anions can direct the ordered assembly of TMCs through directional hydrogen-bonding interactions to construct supramolecular structures, such as N–H···O, C–H···O, etc. [16, 17]. Our research has focused on syntheses of POM-based supramolecular assemblies by utilizing the weak interactions that occur between the surface oxygens of the POMs and TMCs.

An important synthetic strategy for construction of POM-based supramolecular structures rests on the selection of proper ligands. Flexible multi-dentate ligands are usually used in the POM field [18, 19], which induce high-dimensional structures with the linkage of POM–TM–ligand bonds. Rigid chelating organic ligands usually form supramolecular compounds that are constructed by POMs and organic ligands or POMs and TMCs [20]. For example, Lu's group used the organic substrate 2-(3-pyridyl)-benzimidazolium (3-HPBIM) acting as a donor combined with a POM cluster to construct a new optical supramolecular compound [13]. In this work, we chose 2-(4-thiazolyl)benzimidazole (**L**) as the organic component to build POM-based supramolecular structures. This rigid **L** has a thiazolyl and a benzimidazole group (scheme 1), which can offer one S and three N donors. These donors also support hydrogen-bonding interactions with POMs, forming supramolecular structures.

In this work, we have synthesized three supramolecular compounds under hydrothermal conditions, $[Cu^{II}_2Cl(\mathbf{L})_4(PW_{12}O_{40})]\cdot 3H_2O$ (**1**), $[Cu^{II}(\mathbf{L})_2(H_2O)]_2[P_2W_{18}O_{62}]\cdot(H\mathbf{L})_2\cdot 6H_2O$ (**2**), and $[Zn^{II}(\mathbf{L})_3]_4[H(KPW_{12}O_{40})_3]$ (**3**). Furthermore, the electrochemical and photocatalytic properties of these compounds are reported.

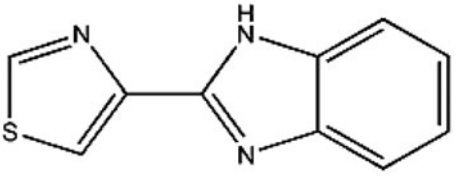

Scheme 1. The ligand 2-(4-thiazolyl)benzimidazole (**L**).

2. Experimental

2.1. *Materials and measurements*

All reagents and solvents for syntheses were purchased from commercial sources and used as received. Elemental analyses were carried out with a Perkin-Elmer 240C elemental analyzer and FT-IR spectra were recorded on a Magna FT-IR 560 spectrometer (KBr pellets). The thermal gravimetric analyses were carried out in N_2 on a Pyris Diamond thermal analyzer with a rate of 10 °C min^{-1}. Electrochemical measurements and data collection were performed with a CHI 440 electrochemical workstation connected to a Digital-586 personal computer. A conventional three-electrode system was used with a saturated calomel electrode as reference electrode and a Pt wire as counter electrode. Chemically bulk-modified carbon paste electrodes (CPEs) were used as the working electrodes. UV/vis absorption spectra were obtained using a SP-1900 UV/vis spectrophotometer.

2.2. *Preparation of the compounds*

2.2.1. Synthesis of $[Cu^{II}_2Cl(L)_4(PW_{12}O_{40})]\cdot 3H_2O$ (1). A mixture of $H_3[PW_{12}O_{40}]\cdot 13H_2O$ (0.15 g, 0.07 mM), $Cu(CH_3COO)_2\cdot 2H_2O$ (0.13 g, 0.6 mM), and **L** (0.13 g, 0.5 mM) was dissolved in 10 mL of distilled water at room temperature. When the pH of the mixture was adjusted to 4.0 with 1.0 M L^{-1} HNO_3, the suspension was put into a Teflon-lined autoclave and kept under autogenous pressure at 160 °C for four days. Dark red crystals were filtered and washed with distilled water (40% yield based on W). Anal. Calcd for $C_{40}H_{34}ClCu_2N_{12}O_{43}PS_4W_{12}$ (3897) (%): C, 12.31; H, 0.76; N, 4.29; Found (%): C, 12.32; H, 0.77; N, 4.31. IR (KBr pellet, cm^{-1}): 3441(s), 2925(w), 1619(m), 1566(w), 1459(w), 1427(w), 1099(s), 971(s), 882(m), 802(s), 706(w), 617(s), 515(s).

2.2.2. Synthesis of $[Cu^{II}(L)_2(H_2O)]_2\{P_2W_{18}O_{62}]\cdot(HL)_2\cdot 6H_2O$ (2). Compound **2** was prepared similarly to **1**, except that $H_6P_2W_{18}O_{62}\cdot 6H_2O$ (0.33 g, 0.11 mM) was used instead of $H_3[PW_{12}O_{40}]\cdot 13H_2O$. Red block-shaped crystals of **2** were obtained in 31% yield (based on W). Anal. Calcd for $C_{60}H_{60}Cu_2N_{18}O_{70}P_2S_6W_{18}$ (5843) (%): C, 12.26; H, 0.87; N, 4.27; Found (%): C, 12.32; H, 0.77; N, 4.31. IR (KBr pellet, cm^{-1}): 3434(s), 2341(w), 1641(m), 1573(w), 1507(m), 1381(w), 1282(w), 1104(s), 957(w), 919(w), 795(m), 713(w), 623(s), 546(w).

2.2.3. Synthesis of $[Zn^{II}(L)_3]_4[H(KPW_{12}O_{40})_3]$ (3). Compound **3** was prepared similarly to **1**, except that $ZnCl_2$ (0.091 g, 0.5 mM) was used instead of $Cu(CH_3COO)_2\cdot 2H_2O$. Yellow black crystals were filtered and washed with distilled water (40% yield based on W). Anal. Calcd for $C_{120}H_{85}K_3N_{36}O_{120}P_3S_{12}W_{36}Zn_4$ (11,424) (%): C, 8.14; H, 1.18; N, 12.65; Found (%): C, 8.09; H, 1.23; N, 12.61. IR (KBr pellet, cm^{-1}): 3442(s), 3066(w), 1633(m), 1506 (w), 1438(w), 1417(w), 1083(s), 969(s), 884(m), 803(s), 706(w), 617(s), 515(s).

2.3. *X-ray crystallographic study*

Crystallographic data for **1**–**3** were collected on a Bruker Smart Apex II diffractometer with Mo Kα ($\lambda = 0.71073$ Å) at 293 K. All the structures were solved by direct methods and

refined on F^2 by full-matrix least squares using the SHELXL package [21]. All hydrogens attached to water were not located, but were included in the structure factor calculations. Detailed crystal data and structure refinement for **1**–**3** are given in table 1. Selected bond lengths and angles are listed in table S1, see online supplemental material at http://dx.doi.org/10.1080/00958972.2014.923847.

3. Results and discussion

3.1. *Description of the crystal structures*

X-ray crystal structure analysis reveals that **1** consists of one Keggin type $[PW_{12}O_{40}]^{3-}$ (abbreviated to PW_{12}) anion, two Cu^{II} ions, one Cl^-, four **L**, and three crystal waters, as shown in figure 1. The PW_{12} presents a classical Keggin anion. The central P atom is surrounded by a cube of eight oxygens with each site half-occupied [17, 22]. The valence sum calculations [23] show that all tungstens are in +VI oxidation states and all coppers are in +II oxidation states.

In **1**, there is one crystallographically independent Cu^{II}. Cu1 is five coordinate with four N from two **L** and one Cl^- in a square pyramidal geometry. The Cu–N bond lengths are 1.946(16)–2.109(18) Å, while the Cu–Cl bond lengths are 2.382(8) and 2.400(7) Å. The angles around Cu^{II} are 80.2(7)–174.8(9)° for N–Cu–N and 88.8(6)–117.5(6)° for N–Cu–Cl. The bond lengths and angles are shown in table S1. **L** with four potential coordination sites (three N and one S) shows a new coordination mode: using two N donors from one thiazole group and one benzimidazole group to fuse one Cu^{II}. **L** is a chelate ligand in **1**. Each Cu^{II} ion is fused by two **L** to form a subunit $\{CuL_2\}^{2+}$. Furthermore, two $\{CuL_2\}^{2+}$ subunits are linked by Cl^- forming a binuclear copper cluster $\{Cu_2L_4Cl\}^{3+}$ with Cl^- as a bridge. This binuclear cluster is the structural feature of **1**. Cl^- bridges forming multi-nuclear structures that are rare especially in POM-based compounds.

Table 1. Crystal data and structure refinement parameters for **1**–**3**.

	1	**2**	**3**
Formula	$C_{40}H_{34}ClCu_2N_{12}O_{43}PS_4W_{12}$	$C_{60}H_{60}Cu_2N_{18}O_{70}P_2S_6W_{18}$	$C_{120}H_{85}K_3N_{36}O_{120}P_3S_{12}W_{36}Zn_4$
Fw	3897	5843	11,424
Crystal system	Monoclinic	Monoclinic	Tetragonal
Space group	*P21/n*	*C2/c*	*P4 cc*
a (Å)	18.261(2)	29.486(6)	23.513(5)
b (Å)	22.099(2)	14.794(3)	23.513(5)
c (Å)	19.389(2)	25.227(5)	19.789(5)
β (°)	98.047(2)	99.819(3)	90
V (Å ^{3})	7747.3(1)	10,843(4)	10,941(4)
Z	4	4	1
D_{Calcd} (g cm^{-3})	3.343	3.58	3.431
μ (mm^{-1})	18.53	19.645	19.503
F (0 0 0)	6976	10,488	9986
R_{int}	0.089	0.0755	0.1129
GOF	0.841	0.908	0.864
R_1[a] [$I > 2\sigma(I)$]	0.0481	0.052	0.0478
wR_2[b] (all data)	0.1603	0.1521	0.1479

[a] $R_1 = \Sigma||F_o| - |F_c||/\Sigma|F_o|$.
[b] $wR_2 = \Sigma[w(F_o^2 - F_c^2)^2]/\Sigma[w(F_o^2)^2]^{1/2}$.

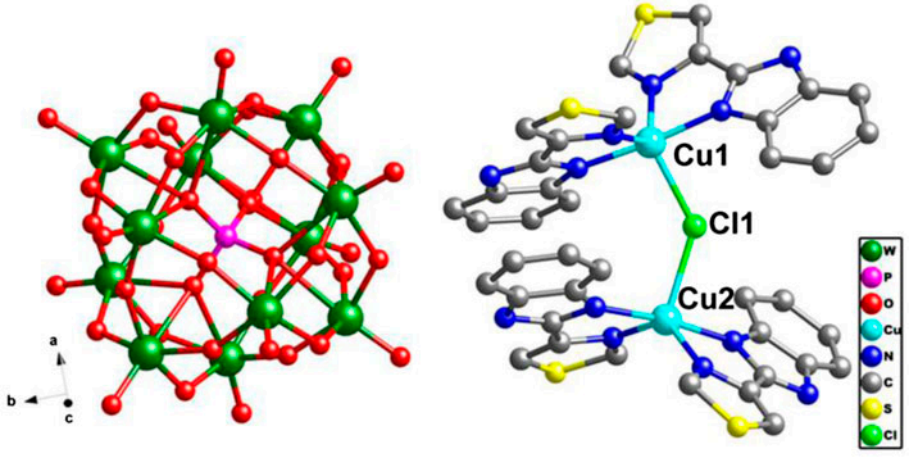

Figure 1. Stick/ball view of **1**. Hydrogens and waters are omitted for clarity.

Though the S in **L** is not utilized to bind Cu^{II} ions, it can be a hydrogen-bonding site connecting with another **L**. Thus, these binuclear clusters connect through weak hydrogen-bonding interactions (C13···S1 = 3.462 Å) to construct a supramolecular chain (figure S1). The PW_{12} anions further offer hydrogen-bonding interactions linking these chains and a 2-D supramolecular network is formed (figure 2).

X-ray crystal structure analysis reveals that **2** consists of one $[P_2W_{18}O_{62}]^{6-}$ (abbreviated to P_2W_{18}) anion, two Cu^{II} ions, four chelating and two discrete **L**, two coordinated and six crystal waters, as shown in figure 3. The P_2W_{18} anion in **2** retains a classical Wells–Dawson structure containing two $[\alpha\text{-A-}PW_9O_{34}]^{9-}$ units from the α-Keggin polyoxoanion by removal of a set of three corner-shared WO_6 octahedra [24]. The P–O and W–O lengths are in the normal ranges. Valence sum calculations [23] show that all tungstens are in the +VI oxidation states and all coppers are +II. To balance the charge of **2**, two protons are added

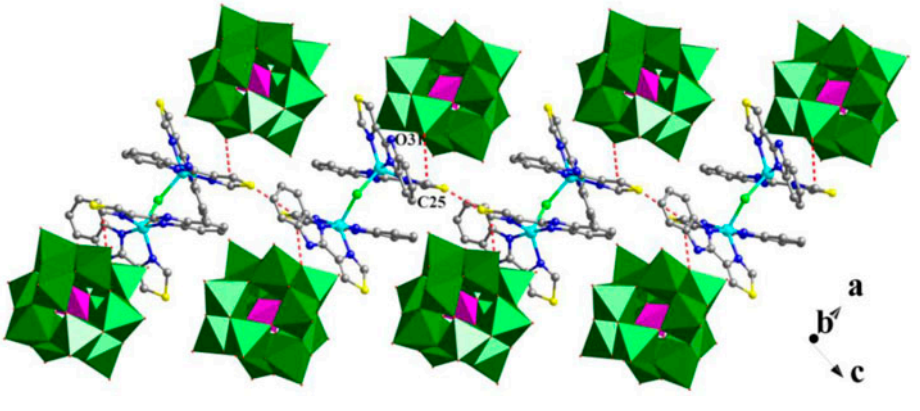

Figure 2. The 2-D supramolecular network of **1**.

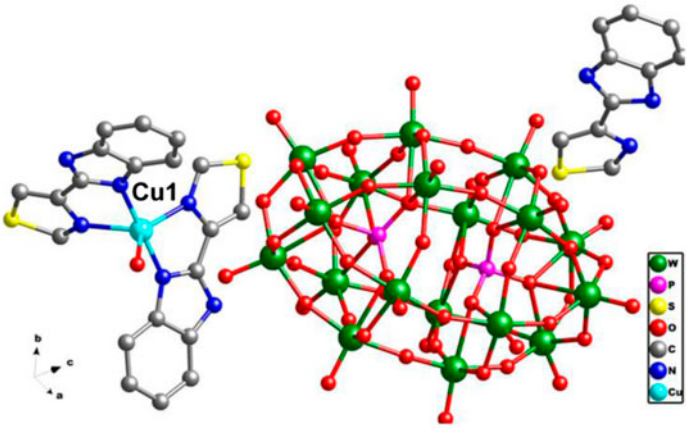

Figure 3. Stick/ball view of the unit of **2**. Hydrogens and waters are omitted for clarity.

to the discrete **L** molecules and **2** is formulated as $[Cu^{II}(\mathbf{L})_2(H_2O)]_2[P_2W_{18}O_{62}]\cdot(H\mathbf{L})_2\cdot 6H_2O$.

In **2**, there is one crystallographically independent Cu^{II} ion. Cu1 is five coordinate with four N from two **L** and one water. The Cu–N bond lengths are 1.927(16)–2.145(15) Å, while the Cu–O bond length is 2.131(15) Å. These bond lengths and angles are shown in table S1. **L** is chelating ligand in **2** by offering two N donors. Each Cu^{II} is coordinated by two **L** and one water, forming a $\{Cu\mathbf{L}_2(H_2O)\}^{2+}$ subunit. The subunits connect with P_2W_{18} anions through hydrogen-bonding interactions between the coordinated water molecules and the O of P_2W_{18} anions (O1 W$\cdots$O19 = 2.938 Å), constructing a 1-D supramolecular chain, as shown in figure 4. The hydrogen-bonding interactions between S of **L** and O of P_2W_{18} anions (S3$\cdots$O13 = 3.185 Å, S2$\cdots$O18 = 3.208 Å) further extend the adjacent chains into a 2-D supramolecular network (figure S2).

X-ray crystal structure analysis reveals that **3** consists of three PW_{12} anions, four Zn^{II} ions, three K^+ ions, and twelve **L**, as shown in figure 5. In PW_{12} anion, the central P atom is surrounded by a cube of eight oxygens with each site half-occupied [17, 22]. Valence sum calculations [23] show that one W is in +V oxidation state and all the Zn atoms are +II. To balance the charge, one proton is added to the anion. The structure of **3** rests on the introduction of K^+. The introduction of alkali metal ions into POM system is rare under hydrothermal conditions [25]. The K^+ ion caps the PW_{12} anion through coordinating with

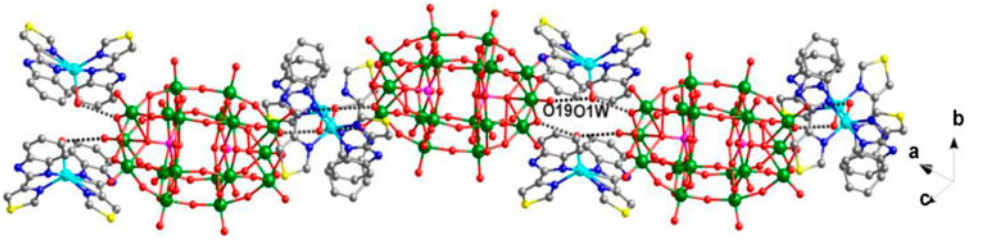

Figure 4. The supramolecular chain of **2**.

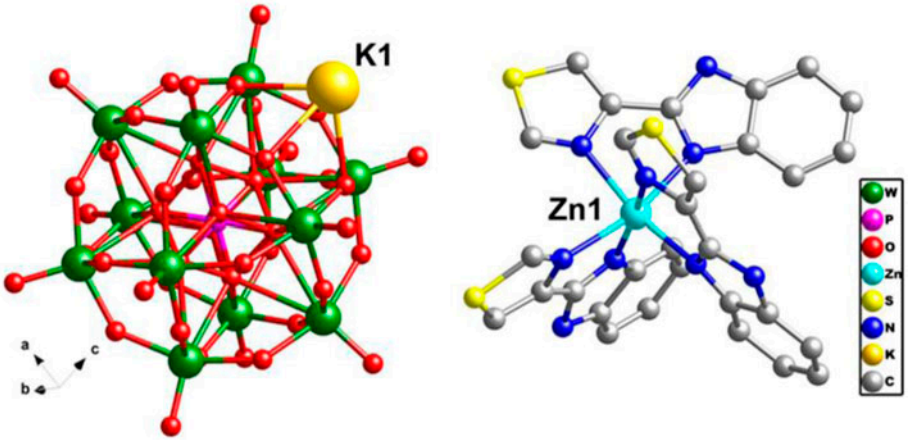

Figure 5. Stick/ball view of **3**. Hydrogens are omitted for clarity.

four oxygens with K–O bond lengths of 2.55(19)–2.651(19) Å. Each PW_{12} anion is bi-capped by two K^+ ions. Thus, a 1-D inorganic chain is formed with the PW_{12} anions and K^+ ions arranging alternately, as shown in figure 6.

In **3**, there is one crystallographically independent Zn^{II} ion. Zn1 is six-coordinate by six N from three **L** in an octahedral geometry. The Zn–N bond lengths are 2.07(2)–2.287(19) Å, while the N–Zn–N angles are 76.7(8)–166.4(7)°. The bond lengths and angles are shown in table S1. **L** still offers two N donors to chelate one Zn^{II} ion. Each Zn^{II} ion is fused by three **L** ligands, forming a discrete subunit $\{Zn\mathbf{L}_3\}^{2+}$. The $\{Zn\mathbf{L}_3\}^{2+}$ subunits connect the POM–K inorganic chains through hydrogen-bonding interactions (N6···O65 = 2.932 Å, C27···O52 = 2.972 Å, C10···O46 = 3.108 Å, S1···O52 = 3.183 Å) and a 3-D supramolecular network is formed (figure 7). There exist 1-D channels along the *c* axis in the 3-D supramolecular framework.

3.2. *FT-IR spectra*

IR spectra of **1**–**3** are shown in figure S3. For **1**, the characteristic bands at 1099, 971, 882, and 802 cm^{-1} are attributed to ν(P–O), ν(W–O_d), and ν(W–$O_{b/c}$–W) of PW_{12}, respectively

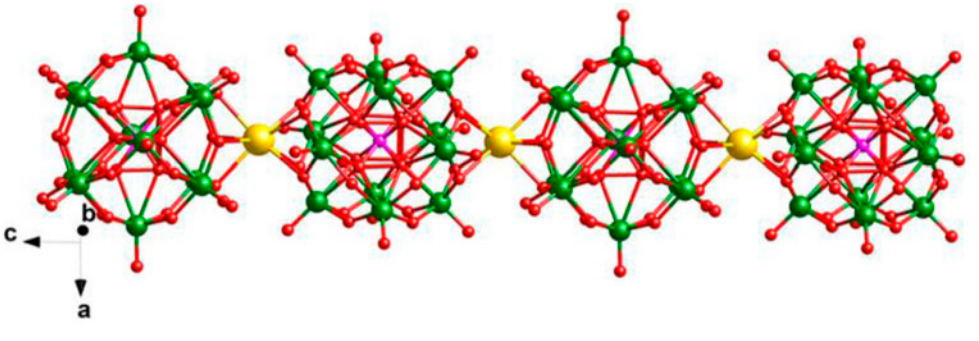

Figure 6. The 1-D inorganic chain of **3**.

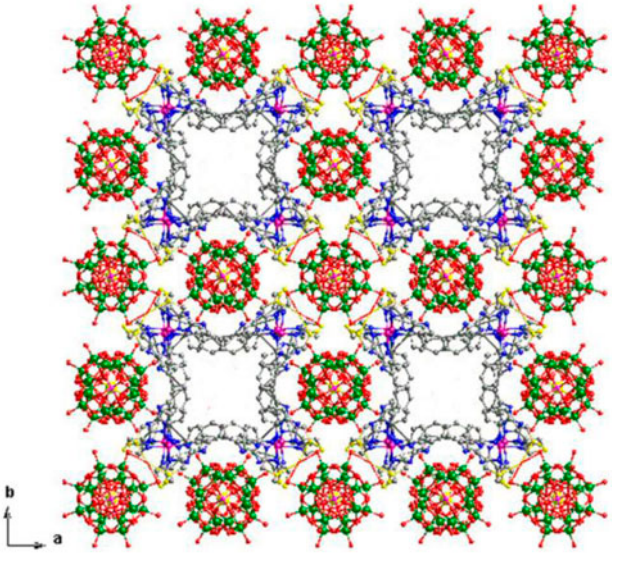

Figure 7. The 3-D supramolecular framework of **3**.

[26]. For **2**, bands at 1104, 957, 919, and 795 cm^{-1} are the characteristic peaks of $\nu(P–O_a)$, $\nu(W–O_d)$, and $\nu(W–O_{b/c}–W)$ of P_2W_{18}, respectively [27]. Characteristic bands at 1083, 969, 884, and 803 cm^{-1} for **3** can be ascribed to $\nu(P–O)$, $\nu(W–O_d)$, and $\nu(W–O_{b/c}–W)$ of PW_{12}, respectively [26]. Furthermore, the characteristic absorptions in the regions of 1427–1619 cm^{-1} for **1**, 1381–1641 cm^{-1} for **2**, and 1417–1633 cm^{-1} for **3** are attributed to the **L** ligands.

3.3. *Thermogravimetric analysis*

The thermogravimetric (TG) analyses of **1**–**3** were carried out in flowing N_2 with a heating rate of 10 °C min^{-1} from 20 to 850 °C, as shown in figure S4. The TG curves of **1** and **2** show two distinct weight loss steps: the first occurs below 300 °C corresponding to loss of water 1.00% (Calcd 1.24%) for **1**, 1.98% (Calcd 1.86%) for **2**. The second weight loss steps in the range of 300–850 °C can be attributed to the loss of organic **L** ligands 24.85% (Calcd 28.53%) for **1** and 20.18% (Calcd 24.59%) for **2**, respectively. The TG curve of **3** shows three distinct weight loss steps attributed to the loss of organic **L** ligands 24.7% (Calcd 24.51%).

3.4. *Electrochemical properties*

Cyclic voltammograms for **1**–CPE in 0.1 M H_2SO_4 + 0.5 M Na_2SO_4 aqueous solution at different scan rates are presented in figure 8(a). From +500 to –780 mV for **1**–CPE, there exist three reversible redox peaks I–I′, II–II′, and III–III′ with the mean peak potentials $E_{1/2} = (E_{pa} + E_{pc})/2$ at –160 (I–I′), –447 (II–II′), and –669 (III–III′) mV (scan rate: 150 mV s^{-1}), respectively. The redox peaks I–I′ and II–II′ correspond to two consecutive one-electron processes of PW_{12}, while III–III′ corresponds to a two-electron process [28].

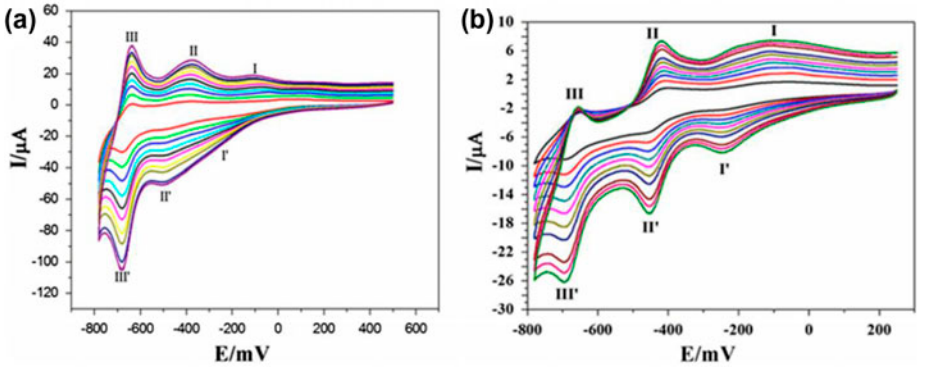

Figure 8. The cyclic voltammograms for **1**– (a) and **2**–CPEs (b) in 0.1 M H_2SO_4 + 0.5 M Na_2SO_4 aqueous solution at different scan rates (from inner to outer: 50, 100, 150, 200, 250, 300, 350, 400, 450, and 500 mV s^{-1}).

The cyclic voltammograms for **2**–CPE in 0.1 M H_2SO_4 + 0.5 M Na_2SO_4 aqueous solution at different scan rates are presented in figure 8(b). Three reversible redox peaks appear in the potential range from +250 to –780 mV for **2**–CPE with the mean peak potentials $E_{1/2} = (E_{pa} + E_{pc})/2$ at –143 (I–I′), –402 (II–II′), and –645 (III–III′) mV (scan rate: 150 mV s^{-1}). These three redox peaks correspond to three consecutive two-electron processes of the W centers in P_2W_{18} [29]. The peak potentials of cyclic voltammograms for **1**– and **2**–CPEs change gradually following the scan rates from 50 to 500 mV s^{-1}: the cathodic peak potentials shift toward the negative direction and the corresponding anodic peak potentials to the positive direction with increasing scan rates.

Figure 9 shows cyclic voltammograms for the electrocatalytic reduction of hydrogen peroxide at **1**–CPE in 0.1 M H_2SO_4 + 0.5 M Na_2SO_4 aqueous solution. With addition of H_2O_2, all three reduction peak currents of **1**–CPE gradually increased while the corresponding oxidation peak currents markedly decreased, suggesting that **1**–CPE shows good electrocatalytic activity toward reduction of H_2O_2. Figure 10 shows cyclic voltammograms for the

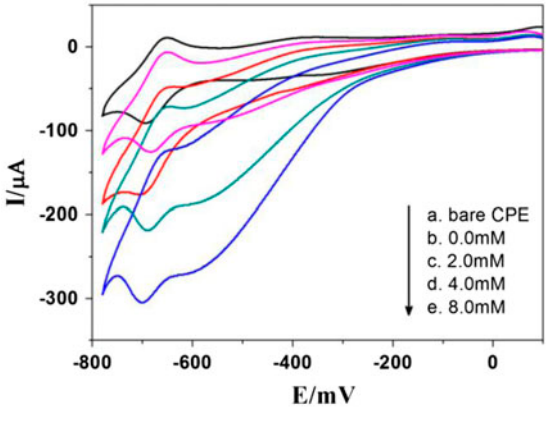

Figure 9. The electrocatalytic reduction of hydrogen peroxide at **1**–CPE containing 0.0–8.0 mM H_2O_2 (a–e). Scan rate: 150 mV s^{-1}.

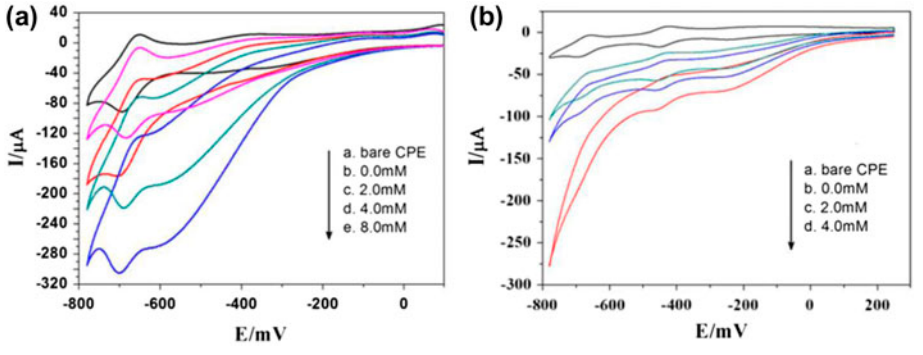

Figure 10. The electrocatalytic reduction of nitrite at **1**– (a) and **2**–CPEs (b) containing 0.0–8.0 mM nitrite (a–e). Scan rate: 150 mV s^{-1}.

electrocatalytic reduction of nitrite at **1**– and **2**–CPEs in 0.1 M H_2SO_4 + 0.5 M Na_2SO_4 aqueous solution. It can be clearly seen that with addition of nitrite, all three reduction peak currents of **1**– and **2**–CPEs gradually increase while the corresponding oxidation peak currents decrease, which indicates that the three reduced species of the polyoxoanions in both CPEs show good electrocatalytic activities toward reduction of nitrite.

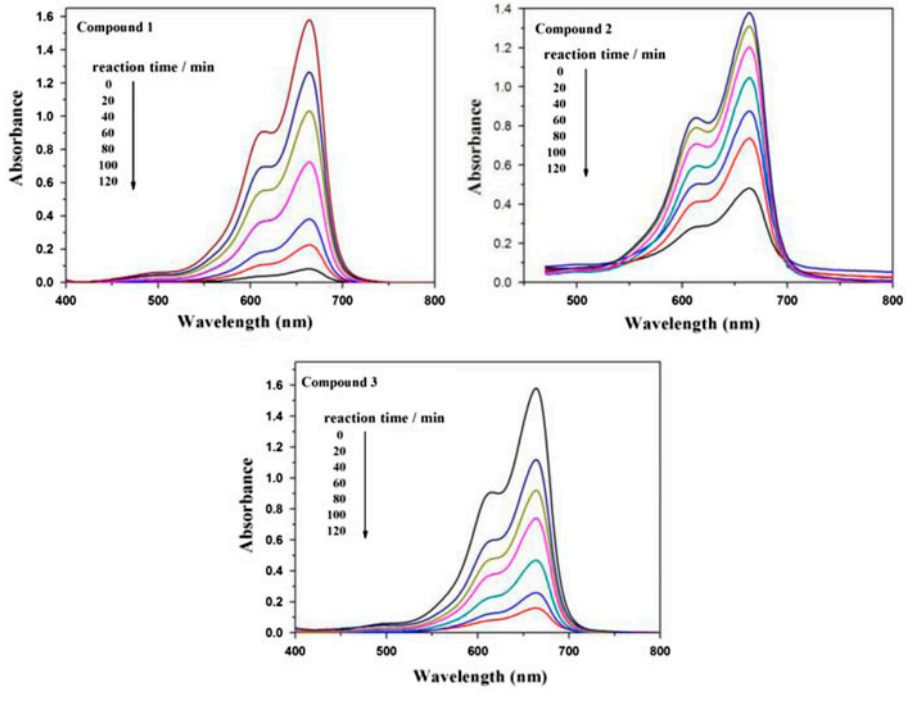

Figure 11. The photocatalytic activities of **1–3**.

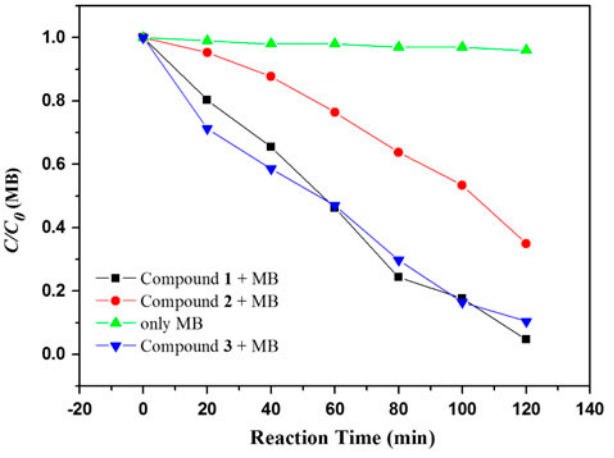

Figure 12. Photocatalytic decomposition rate of MB solution under UV irradiation with **1–3** and only MB.

3.5. *Photocatalytic properties*

Some POM-based compounds exhibit photocatalytic activities to degrade organic dyes [30, 31]. In this work, we investigated the photocatalytic activities of **1**–**3** for degradation of methylene blue (MB) solution under UV irradiation from a Hg lamp, as shown in figure 11. First, 100 mg of compound was suspended in 0.02 mM L^{-1} MB aqueous solution (250 mL) and magnetically stirred for about 10 min to ensure equilibrium in the dark. Then, 5.0 mL samples were taken out every 20 min for analysis by UV–visible spectroscopy. It can be clearly observed that the absorbance peak of MB decreased from 1.57 to 0.07 for **1**, 1.38 to 0.48 for **2,** and 1.58 to 0.16 for **3** after 120 min. The calculations reveal that conversions of MB are 95.1% for **1**, 65.4% for **2,** and 89.4% for **3**. The results indicate that all three compounds show excellent photocatalytic activities for degradation of MB, especially **1**. Absorption peaks of MB decreased with increasing reaction time (figure 12).

4. Conclusion

Three POM-based supramolecular compounds have been obtained under hydrothermal conditions. Compound **1** shows a 2-D supramolecular structure constructed from $\{Cu_2\mathbf{L}_4Cl\}^{3+}$ subunits and PW_{12} anions. Compound **2** exhibits a 1-D supramolecular chain built by P_2W_{18} anions and $[Cu\mathbf{L}_2(H_2O)]^{2+}$. The 3-D supramolecular framework of **3** contains discrete $[Zn^{II}(\mathbf{L})_3]^{2+}$ subunits and 1-D PW_{12} chains linked by K^+ ions. These three compounds show good electrochemical and photocatalytic properties. Further study on other new ligands with more supramolecular synthons is underway.

Supplementary material

Crystallographic data for the structures reported in this article have been deposited in the Cambridge Crystallographic Data Center with CCDC numbers 969782–969784.

Funding

Financial supports of this research by the National Natural Science Foundation of China [grant number 21171025], [grant number 21101015], [grant number 21201021]; New Century Excellent Talents in University [grant number NCET-09-0853]; Program of Innovative Research Team in the University of Liaoning Province [grant number LT2012020]; Talent-supporting Program Foundation of Education Office of Liaoning Province [grant number LJQ2012097]; Undergraduate Scientific and Technological Innovation Project of Liaoning Province [grant number 20131016702].

References

[1] H.N. Miras, C.J. Richmond, D.L. Long, L. Cronin. *J. Am. Chem. Soc.*, **134**, 3816 (2012).
[2] Y. Hou, M. Nyman, M.A. Rodriguez. *Angew. Chem. Int. Ed.*, **50**, 12514 (2011).
[3] Z.Y. Zhang, Q.P. Lin, D. Kurunthu, T. Wu, F. Zuo, S.T. Zheng, C.J. Bardeen, X.H. Bu, P.Y. Feng. *J. Am. Chem. Soc.*, **133**, 6934 (2011).
[4] X.L. Wang, Y.F. Bi, B.K. Chen, H.Y. Lin, G.C. Liu. *Inorg. Chem.*, **47**, 2442 (2008).
[5] D. Li, J. Song, P. Yin, S. Simotwo, A.J. Bassler, Y.Y. Aung, J.E. Roberts, K.I. Hardcastle, C.L. Hill, T. Liu. *J. Am. Chem. Soc.*, **133**, 14010 (2011).
[6] X.L. Wang, C. Qin, E.B. Wang, Z.M. Su, Y.G. Li, L. Xu. *Angew. Chem. Int. Ed.*, **45**, 7411 (2006).
[7] Y.F. Bi, S.C. Du, W.P. Liao. *Chem. Commun.*, **47**, 4724 (2011).
[8] A.X. Tian, X.L. Lin, Y.J. Liu, G.Y. Liu, J. Ying, X.L. Wang, H.Y. Lin. *J. Coord. Chem.*, **65**, 2147 (2012).
[9] J.Y. Guo, X.F. Jin, L. Chen, Z.X. Wang, Y. Xu. *J. Coord. Chem.*, **65**, 3821 (2012).
[10] C. Liang, Y. Lu, H. Fu, W.L. Chen, E.B. Wang. *J. Coord. Chem.*, **65**, 3254 (2012).
[11] Y.L. Xu, K. Yu, B.B. Zhou, Z.H. Su, J. Wu. *J. Coord. Chem.*, **66**, 1303 (2013).
[12] Y. Wang, C.L. Pan, L.N. Xiao, F.Q. Wu, H. Ding, Y.B. Liu, Z.M. Gao, D.F. Zheng, T.G. Wang, G.D. Yang, X.B. Cui, J.Q. Xu. *J. Solid State Chem.*, **183**, 2862 (2010).
[13] Y.M. Xie, Q.S. Zhang, Z.G. Zhao, X.Y. Wu, S.C. Chen, C.Z. Lu. *Inorg. Chem.*, **47**, 18 (2007).
[14] F.J. Ma, S.X. Liu, C.Y. Sun, D.D. Liang, G.J. Ren, F. Wei, Y.G. Chen, Z.M. Su. *J. Am. Chem. Soc.*, **10**, 1021 (2010).
[15] E. Coronado, J.R. Galán-Mascarós, C. Giménez-Saiz, C.J. Gómez-García, E. Martínez-Ferrero, M. Almeida, E.B. Lopes. *Adv. Mater.*, **16**, 324 (2004).
[16] Z.G. Han, Q.X. Zhang, Y.Z. Gao, J.J. Wu, X.L. Zhai. *Dalton Trans.*, 1332 (2012).
[17] L.N. Xiao, Y. Wang, C.L. Pan, J.N. Xu, T.G. Wang, H. Ding, Z.M. Gao, D.F. Zheng, X.B. Cui, J.Q. Xu. *CrystEngComm.*, **10**, 1039 (2010).
[18] C. Qin, X.L. Wang, E.B. Wang, Z.M. Su. *Inorg. Chem.*, **47**, 55555 (2008).
[19] X.L. Wang, H.L. Hu, G.C. Liu, H.Y. Lin, A.X. Tian. *Chem. Commun.*, **46**, 6485 (2010).
[20] Z.G. Han, Y.N. Wang, J.J. Wu, X.L. Zhai. *Solid State Chem.*, **13**, 1560 (2011).
[21] (a) G.M. Sheldrick. *SHELXS-97*, University of Göttingen, Göttingen (1997); (b) G.M. Sheldrick. *Acta Crystallogr., Sect. A*, **64**, 112 (2008).
[22] Y. Bai, G.Q. Zhang, D.B. Dang, P.T. Ma, H. Gao, J.Y. Niu. *CrystEngComm.*, **10**, 1039 (2011).
[23] I.D. Brown, D. Altermatt. *Acta Crystallogr., Sect. B: Struct. Sci.*, **41**, 244 (1985).
[24] J.Q. Sha, J. Peng, Y.Q. Lan, Z.M. Su, H.J. Pang, A.X. Tian, P.P. Zhang, M. Zhu. *Inorg. Chem.*, **47**, 5145 (2008).
[25] J. Li, Y. Huang, Q.X. Han. *J. Coord. Chem.*, **66**, 2405 (2013).
[26] Y.N. Chi, F.Y. Cui, A.R. Jia, X.Y. Ma, C.W. Hu. *CrystEngComm.*, **14**, 3183 (2012).
[27] A.X. Tian, J. Ying, J. Peng, J.Q. Sha, Z.G. Han, J.F. Ma, Z.M. Su, N.H. Hu, H.Q. Jia. *Inorg. Chem.*, **47**, 3274 (2008).
[28] A.X. Tian, J. Ying, J. Peng, Z.M. Su, H.J. Pang, P.P. Zhang, Y. Chen, M. Zhu, Y. Shen. *Cryst. Growth Des.*, **10**, 1104 (2010).
[29] P.P. Zhang, J. Peng, H.J. Pang, J.Q. Sha, M. Zhu, D.D. Wang, M.G. Liu. *CrystEngComm.*, **13**, 3832 (2011).
[30] J. Lü, J.X. Lin, X.L. Zhao, R. Cao. *Chem. Commun.*, **47**, 761 (2011).
[31] H.J. Pang, H.Y. Ma, J. Peng, C.J. Zhang, P.P. Zhang, Z.M. Su. *CrystEngComm.*, **13**, 7079 (2011).